evaporated to afford **36b**. The residue was dissolved in water (2 mL) and stirred for 30 min under a hydrogen atmosphere (1 atm) with Lindlar catalyst (50 mg). The mixture was filtered through Celite and concentrated to afford hikizimycin (5.4 mg, quant): $[\alpha]^{23}_D = -13°$ (*c* 0.53, H_2O); ^1H NMR (D_2O, 500 MHz) δ 2.65 (t, J = 9.8 Hz, 1 H, C3″H), 2.90 (t, J = 9.8 Hz, 1 H, C4′H), 3.12 (dd, J = 7.8, 10.0 Hz, 1 H, C2″H), 3.16 (t, J = 9.7 Hz, 1 H, C4″H), 3.33 (m, 1 H, C5″H), 3.40 (t, J = 9.3 Hz, 1 H, C3′H), 3.52 (dd, J = 6.2, 11.7 Hz, 1 H, C11′H), 3.61 (m, 4 H), 3.71 (dd, J = 2.6, 11.7 Hz, 1 H, C11′H), 3.77 (~d, 2 H, C5′+7′H), 3.86 (d, J = 9.8 Hz, 1 H), 4.19 (d, J = 4.4 Hz, 1 H), 4.49 (d, J = 7.8 Hz, 1 H, C1″H), 5.43 (d, J = 9.4 Hz, 1 H, C1′H), 5.94 (d, J = 7.5 Hz, 1 H, vinylic), 7.56 (d, J = 7.6 Hz, 1 H, vinylic); ^{13}C NMR (D_2O, 100.6 MHz) δ 53.14, 57.14, 60.60, 63.02, 67.59, 68.61, 68.67, 69.09, 70.60, 71.02, 72.99, 76.49, 76.90, 78.21, 79.41, 83.59, 96.62, 103.84, 141.70, 157.66, 165.73; IR (film) 2246 (br), 2925 (m), 2854 (w), 1654 (s), 1604 (m), 1497 (m), 1379 (w), 1291 (w), 1212 (w), 1074 (s), 784 (w); MS (FAB) 584 (M + 1, 5.2), 606 (M + Na, 5.8), 185 (100); HRMS (FAB) m/z 584.2432 (calcd 584.2416 for $C_{21}H_{37}N_5O_{14}$ + H).

Peracetylhikizimycin. Natural hikizimycin (0.043 g, 0.074 mmol) was stirred in acetic anhydride (0.7 mL) and pyridine (0.6 mL) containing DMAP (cat.). The mixture was allowed to stir for 6 days with occasional sonication. The mixture was evaporated, and the residue was purified by flash chromatography with ethyl acetate to 10–20% methanol–ethyl acetate to afford the peracetate (0.064 g, 77%). Synthetic hikizimycin was acetylated in a similar manner: ^1H NMR ($CDCl_3$, 250 MHz) δ 1.8–2.3 (s, CH_3), 3.7 (d, 1 H), 4.0 (m, 4 H), 4.2 (d, 1 H), 4.3 (m, 2 H), 4.7 (br, 1 H), 4.8 (t, 1 H), 4.9 (t, 1 H), 5.1 (m, 3 H), 5.3 (m, 4 H), 6.0 (d, 2 H), 6.9 (br, 1 H), 7.5 (d, 1 H), 7.9 (d, 1 H), 9.0 (br, 1 H), peak positions were variable; ^{13}C NMR ($CDCl_3$, 75.5 MHz) δ 20.12, 20.50, 20.77, 20.85, 20.94, 21.11, 22.73, 22.90, 24.76, 50.17, 53.44, 61.72, 62.10, 67.50, 67.90, 68.13, 68.40, 68.96, 70.00, 71.76, 73.01, 73.89, 74.21, 81.13, 81.31, 97.30, 101.85, 145.78, 155.01, 162.91, 169.27, 169.54, 169.86, 170.00, 170.08, 170.16, 170.36, 170.46, 171.16, 171.24; IR (neat) 3316 (br), 2986 (w), 1750 (s), 1684 (m), 1489 (m), 1372 (m), 1223 (s), 1044 (m).

Acknowledgment. We thank the NIGMS (GM-38627) and Pfizer for their support of this research and Dr. R. Nagarajan (Lilly Research Laboratories) for a gift of natural hikizimycin.

Supplementary Material Available: Spectral data of the natural and synthetic hikizimycins as well as their peracetates (5 pages). Ordering information is given on any current masthead page.

Dynamics of the Reactions of [*meso*-Tetrakis(2,6-dimethyl-3-sulfonatophenyl)porphinato]-manganese(III) Hydrate with Various Alkyl Hydroperoxides in Aqueous Solution. Product Studies and Comparison of Kinetic Parameters

Ramesh D. Arasasingham,† Seungwon Jeon, and Thomas C. Bruice*

Contribution from the Department of Chemistry, University of California at Santa Barbara, Santa Barbara, California 93106. *Received August 26, 1991*

Abstract: The second-order rate constants (k_{ly}) for reactions of [*meso*-tetrakis(2,6-dimethyl-3-sulfonatophenyl)porphinato]manganese(III) hydrate [(**1**)$Mn^{III}(X)_2$, X = H_2O or HO^-] with *t*-BuOOH and (Ph)(Me)$_2$COOH have been determined in aqueous solution in the pH range 7.3–12.6. The pH dependencies of k_{ly} were fitted to a kinetic expression (eq 2) that was similar to that shown previously to describe the pH dependence of the reaction of (**1**)$Mn^{III}(X)_2$ with (Ph)$_2$(MeOCO)COOH. Comparison of the very similar pH–rate profiles for *t*-BuOOH, (Ph)(Me)$_2$COOH, and (Ph)$_2$(MeOCO)COOH (ROOH) showed that the log of the second-order rate constants exhibits only a modest dependency on the acidity of the ROH leaving group (–0.32 for the pH 7.3–10.0 range) as would be expected of a homolytic reaction. Product analysis on the reactions with *t*-BuOOH in the absence of the ABTS trapping agent provided (Me)$_2$CO (60–70%) as the major product with the remainder of the oxidant recovered as *t*-BuOH (12%), *t*-BuOOMe, (*t*-BuO)$_2$, MeOH, and HCHO. The product distributions showed no significant dependence on the pH of the reaction solutions. In the presence of ABTS (Me)$_2$CO is formed in 5% yield, and the main product is *t*-BuOH (89%). These findings are consistent with a mechanism involving the homolytic (but not heterolytic) cleavage of the O–O bond of manganese(III)-coordinated alkyl hydroperoxide. Addition of imidazole to the reaction of (**1**)$Mn^{III}(X)_2$ with *t*-BuOOH resulted in a ~4–10-fold enhancement in the rate of reaction. The pH dependence of log k_{Im} for the reaction in the presence of imidazole, from pH 5.3 to 12.6, was found to be in accord with that determined previously for (Ph)$_2$-(MeOCO)COOH. The product distribution for the reactions in the presence of imidazole showed significant dependence on the pH of the reaction mixtures. At pH 7.8 and 10.0 the product profiles were only consistent with a homolytic mechanism for the O–O bond cleavage where the major product was (Me)$_2$CO (63–67%), with the remainder being *t*-BuOH (19%), *t*-BuOOMe (13–16%), (*t*-BuO)$_2$, MeOH, and HCHO. At pH 12.6, the yield of *t*-BuOH (63%) increased dramatically with concomitant decreases in the yields of (Me)$_2$CO (34%), *t*-BuOOMe (4%), (*t*-BuO)$_2$, MeOH, and HCHO. The latter product distribution finds explanation in a change in mechanism of the O–O bond cleavage from homolysis to heterolysis as a result of the proton dissociation of the manganese(III)-coordinated ImH (i.e., (**1**)Mn^{III}(OOR)(ImH) → [(**1**)Mn^{III}(OOR)(Im)]$^-$). The acidity dependences of the 1e$^-$ oxidation and reduction potentials of (**1**)Mn^{III}(X)(ImH) have been used to determine the acid ionization constants for the mono-imidazole-ligated (**1**)$Mn^{II}(H_2O)$(ImH), (**1**)$Mn^{III}(H_2O)$(ImH), and (**1**)$Mn^{IV}(H_2O)$(ImH) species. The change in 1e$^-$ oxidation potentials with pH has also been compared to the change in rate constants with pH for reactions occurring in the presence and absence of imidazole.

Introduction

Redox reactions involving manganese are of significance in a number of biochemical systems. Manganese is known to participate in the oxidation of water to molecular oxygen in photosystem II of green plant photosynthesis[1] as well as in certain catalases,[2] peroxidases,[3] and superoxide dismutase enzymes.[4] Low molecular weight complexes of manganese have also been shown

† Present address: Department of Chemistry, Murray State University, Murray, KY 42071.

(1) (a) Renger, G. *Angew. Chem., Int. Ed. Engl.* **1987**, *26*, 643. (b) Dismukes, G. C. *Photochem. Photobiol.* **1986**, *43*, 99. (c) Renger, G.; Govindjee *Photosynth. Res.* **1985**, *6*, 33. (d) Livorness, J.; Smith, T. D. *Struct. Bonding* **1982**, *48*, 1. (e) Kok, B.; Forbush, B.; McGloin, M. *Photochem. Photobiol.* **1970**, *11*, 457.

0002-7863/92/1514-2536$03.00/0

to protect cells from damage by oxygen toxicity.[5] Further, reconstitution of the apoenzyme of horseradish peroxidase with manganese protoporphyrin has been reported to provide partial restoration of peroxidase activity.[6] Related synthetic manganese porphyrin complexes have also been shown to be very versatile catalysts for the oxidation of a wide variety of organic substrates that include alkanes, alkenes, alcohols, ethers, and amines.[7]

In a preceding paper[8] we described the dynamics of the reactions of the water soluble and non μ-oxo dimer forming [*meso*-tetrakis(2,6-dimethyl-3-sulfonatophenyl)porphinato]manganese(III) hydrate [(**1**)$Mn^{III}(X)_2$, X = H_2O or HO^-] with the reactive hydroperoxide, $(Ph)_2(MeOCO)COOH$, in the presence and absence of imidazole. The behavior of (**1**)$Mn^{III}(X)_2$ was compared to that of the related and much more intensively studied (**1**)$Fe^{III}(X)_2$ which catalyze the homolytic cleavage of the O–O bond of alkyl hydroperoxides after formation of a hydroperoxide-coordinated iron(III) species.[9] For (**1**)$Mn^{III}(X)_2$ in the absence of imidazole, the kinetics of the reaction were shown to display pH dependence consistent with a scheme involving the critical formation of two hydroperoxide-coordinated manganese(III) intermediates at different pH values. A kinetic expression describing the pH dependence of the second-order rate constants for the bimolecular reactions of hydroperoxides with Mn(III) porphyrins was derived from Scheme I with the assumption of a steady state in the intermediates IV and V. A similar expression was derived for the reactions in the presence of imidazole (Scheme II) which displayed pH dependence consistent with the steady state formation of hydroperoxide-coordinated manganese(III) imidazole intermediates IX, X, and XI. However, a definitive mechanism for the O–O bond-breaking step of the hydroperoxide-coordinated manganese could not be established since product studies on these reactions were complicated by the instability of the alcohol product and the reactivity of the hydroperoxide $(Ph)_2(MeOCO)COOH$.

The present work is concerned with gaining an understanding of the mechanism for the O–O bond-breaking step in the decomposition of manganese(III) porphyrin–hydroperoxide complexes in water in the presence and absence of imidazole. To this end, product studies as well as kinetic studies on the pH dependence of the second-order rate constants for the reactions of *t*-BuOOH and $(Ph)(Me)_2COOH$ with (**1**)$Mn^{III}(X)_2$ have been carried out and compared with the results from the previous study with $(Ph)_2(MeOCO)COOH$. Additionally, the acid ionization constants for the mono-imidazole-ligated species (**1**)$Mn^{II}(H_2O)(ImH)$, (**1**)$Mn^{III}(H_2O)(ImH)$, and (**1**)$Mn^{IV}(H_2O)(ImH)$ have been determined from the acidity dependences of the potentials for the 1e$^-$ oxidation and reduction of (**1**)$Mn^{III}(X)(ImH)$. The change in 1e$^-$ oxidation potentials with pH has also been compared to the change in rate constants with pH for reactions occurring in the presence and absence of imidazole.

Scheme I

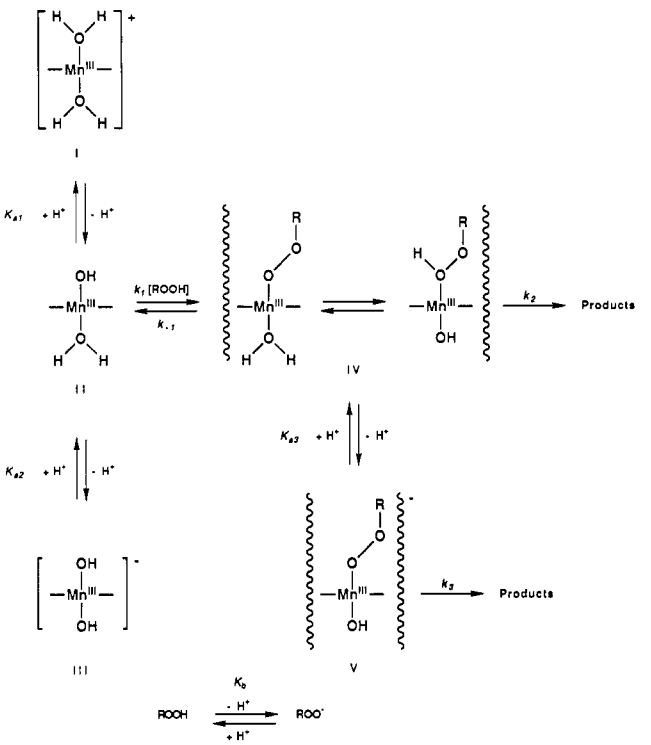

Experimental Section

Materials. Deionized, double-glass distilled water was used for all experiments. The disodium salt of 2,2′-azinobis(3-ethylbenzthiazoline)sulfonic acid (ABTS) was prepared[9g] from the diammonium salt (Sigma Chemical Co.). The *t*-BuOOH (70% w/w) and $(Ph)(Me)_2COOH$ were purchased from Aldrich Chemical Co., and their purity was determined by iodometric analysis[10] prior to use. Imidazole was twice recrystallized from benzene. All the buffer and salt solutions were prepared from reagent-grade chemicals and passed through a Chelex 100 column or extracted with 0.01% dithiazone in dichloromethane to remove possible heavy-metal contaminants. The (**1**)$Mn^{III}(X)_2$ was from a previous study.[8]

Instrumentation. Kinetic studies and absorption measurements were conducted using either a Perkin-Elmer 553 spectrophotometer or a Cary 14 spectrophotometer interfaced to a Zenith computer equipped with OLIS (On-Line Instrument System Inc.). The cell compartments were thermostated at 30 °C. A Hewlett-Packard 9825A computer, equipped with a 9864A digitizer and plotter, was employed for the analysis of the kinetic traces and pH–rate profiles, with the appropriate software programs written for these purposes. pH measurements were carried out with a Radiometer Model pH M26 with metrohm electrode. The GC analyses were performed with a Varian 3700 series gas chromatograph equipped with a flame ionization detector and interfaced to a Hewlett Packard HP3392A integrator. The separation of products in aqueous solution was achieved by on-column injection to a SGE, QC3/BP-1 (25 × 0.32 mm i.d.) capillary column at 35 °C. Cyclic voltammetric measurements were accomplished with a Bioanalytical Systems Model CV-27 potentiostat and a Houston Instruments Model 100 Omnigraphic recorder. A platinum flag electrode separated from the analyte compartment by a medium porosity frit was used as the auxiliary electrode. An Ag/AgCl electrode (filled with aqueous tetramethylammonium chloride solution and standardized to 0.00 V vs SCE[11]) with a solution junction via a Pyrex-glass tube closed with a cracked-glass bead (soft glass) and contained in a luggin capillary was used as the reference electrode. A glassy carbon (2.8-mm diameter) was employed as the working electrode for the determination of the pH dependence of po-

(2) (a) Beyer, W. F.; Fridovich, I. In *Oxygen Radicals in Biology and Medicine*; Simic, M. G., Taylor, K. A., Ward, J. F., von Sanntag, C., Eds.; Plenum: New York, 1988; p 651. (b) Beyer, W. F.; Fridovich, I. *Biochemistry* **1985**, *24*, 6460. (c) Kono, Y.; Fridovich, I. *J. Biol. Chem.* **1983**, *258*, 6015. (d) Fronko, R. M.; Penner-Hahn, J. E.; Bender, C. J. *J. Am. Chem. Soc.* **1988**, *110*, 7554.

(3) For reviews, see: (a) Schoemaker, H. E. *Recl. Trav. Chim. Pays-Bas* **1990**, *109*, 255. (b) Guengerich, F. P. *Crit. Rev. Biochem. Mol. Biol.* **1990**, *25*, 97. (c) Gold, M. H.; Wariishi, H.; Valli, K. *ACS Symp. Ser.* **1989**, *389*, 127.

(4) Michaelson, A. M.; McCord, J. M.; Fridovich, I., Eds. *Superoxide and Superoxide Dismutases*; Academic Press: New York, 1977.

(5) Archibald, F. S.; Fridovich, I. *Arch. Biochem. Biophys.* **1982**, *214*, 452. (b) Kono, Y.; Takahashi, M. A.; Asada, K. *Arch. Biochem. Biophys.* **1976**, *174*, 452.

(6) Yonetani, T.; Asakura, T. *J. Biol. Chem.* **1969**, *244*, 4580.

(7) For a review, see: (a) Holm, R. H. *Chem. Rev.* **1987**, *87*, 1401.

(8) Arasasingham, R. D.; Bruice, T. C. *J. Am. Chem. Soc.* **1991**, *113*, 6095.

(9) (a) Bruice, T. C.; Zipplies, M. F.; Lee, W. A. *Proc. Natl. Acad. Sci., U.S.A.* **1986**, *83*, 4646. (b) Zipplies, M. F.; Lee, W. A.; Bruice, T. C. *J. Am. Chem. Soc.* **1986**, *108*, 4433. (c) Lindsay Smith, J. R.; Balasubramanian, P. N.; Bruice, T. C. *J. Am. Chem. Soc.* **1988**, *110*, 7411. (d) Bruice, T. C.; Balasubramanian, P. N.; Lee, R. W.; Lindsay Smith, J. R. *J. Am. Chem. Soc.* **1988**, *110*, 7890. (e) Balasubramanian, P. N.; Lindsay Smith, J. R.; Davies, M. J.; Kaaret, T. W.; Bruice, T. C. *J. Am. Chem. Soc.* **1989**, *111*, 1477. (f) Balasubramanian, P. N.; Lee, R. W.; Bruice, T. C. *J. Am. Chem. Soc.* **1989**, *111*, 8714. (g) Panicucci, R.; Bruice, T. C. *J. Am. Chem. Soc.* **1990**, *112*, 6063. (h) Murata, K.; Panicucci, R.; Gopinath, E.; Bruice, T. C. *J. Am. Chem. Soc.* **1990**, *112*, 6072. (i) Gopinath, E.; Bruice, T. C. *J. Am. Chem. Soc.* **1991**, *113*, 4657. (j) Gopinath, E.; Bruice, T. C. *J. Am. Chem. Soc.* **1991**, *113*, 6090.

(10) Bruice, T. C.; Noar, J. B.; Ball, S. S.; Venkataram, U. V. *J. Am. Chem. Soc.* **1983**, *105*, 2452.

(11) Sawyer, D. T.; Roberts, J. L., Jr. *Experimental Electrochemistry for Chemists*; Wiley: New York, 1974; p 44.

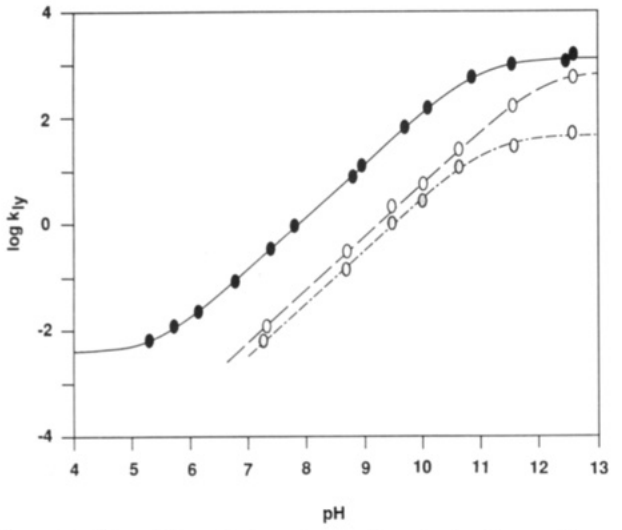

Figure 1. Plots of the pH dependence of log k_{ly} for the reactions of (**1**)$Mn^{III}(X)_2$ (X = H_2O or HO^-) with *t*-BuOOH (hatched oval), (Ph)(Me)$_2$COOH (open oval), and (Ph)$_2$(MeOCO)COOH (solid oval). The points are experimentally determined rate constants and the lines were computer generated by iterative fitting of the points to the appropriate equation (Results). The values of constants that provided the optimal fits are provided in Table I.

Table I. Values of Rate and Equilibrium Constants Obtained from the Fitting of Equation 2 to the Experimental Points for the Reactions of (**1**)$Mn^{III}(X)_2$ with *t*-BuOOH and (Ph)(Me)$_2$COOH in Figure 1 (30 °C and μ = 0.2 with $NaNO_3$)

equiv kinetic terms	*t*-BuOOH	(Ph)(Me)$_2$COOH
k_aK_a (s^{-1})	5.81×10^{-10}	3.23×10^{-10}
K_a (M^{-1})	6.96×10^{-12}	7.83×10^{-13}

tentials in aqueous solution. All working electrode surfaces were highly polished with Al_2O_3 paste prior to each experiment. The reproducibility of individual potential values was ±5 mV. All reported potentials are with respect to saturated calomel electrode (SCE).

Results

The reactions of (1)$Mn^{III}(X)_2$ with *t*-BuOOH and (Ph)(Me)$_2$COOH (30 °C; μ = 0.2 with $NaNO_3$; pH 7.3–12.6) were monitored by following the oxidation of the ABTS trapping agent, {disodium 2,2′-azinobis(3-ethylbenzthiazoline)sulfontate}, to $ABTS^{\cdot+}$ at 660 nm (eq 1).[8] A typical reaction mixture contained

$$ROOH + 2ABTS \xrightarrow{(1)Mn^{III}(X)_2} ROH + HO^- + 2ABTS^{\cdot+} \quad (1)$$

a buffered solution of (**1**)$Mn^{III}(X)_2$ in concentrations ranging from 5.3×10^{-6} to 5.3×10^{-5} M with 1.0×10^{-2} M ABTS. Buffers employed were $H_2PO_4^-/HPO_4^{2-}$ (pH 7.3), HCO_3^-/CO_3^{2-} (pH 8.7–10.6), and H_2O/HO^- (pH 10.6 and above). The reactions were initiated by addition of hydroperoxide to a final concentration of 9.6×10^{-5} M {for *t*-BuOOH} and 8.3×10^{-5} M {for (Ph)(Me)$_2$COOH}. The fitting of the kinetic data, in order to determine the apparent first-order rate constants (k_{obsd}) for ABTS → $ABTS^{\cdot+}$, was carried out as described previously using five to six values of [(**1**)$Mn^{III}(X)_2$] which spanned a 10-fold concentration range. At all pH values examined, k_{obsd} was found to be linearly dependent on [(**1**)$Mn^{III}(X)_2$]. Below pH 7.3, the reactions were found to be so slow that values of k_{obsd} were obtained by the method of initial rates while between pH 7.3 and 9.5 k_{obsd} was obtained by fitting of absorbance readings with time to the first-order rate law. Above pH 9.5 the rate constants were obtained by fitting the changes in absorbance to the rate expression for two sequential first-order reactions (ABTS → $ABTS^{\cdot+}$ → $ABTS^{2+}$).[8] The pH-dependent second-order rate constants (k_{ly}) for reaction of hydroperoxide with manganese(III) porphyrin were obtained as slopes of the linear plots of k_{obsd} vs [(**1**)$Mn^{III}(X)_2$] at constant pH values. The pH dependence of k_{ly} for the reaction of (**1**)$Mn^{III}(X)_2$ with *t*-BuOOH and (Ph)(Me)$_2$COOH is shown in Figure 1, where the experimental points were fit to the empirical eq 2 (standard error for *t*-BuOOH = 6.61×10^{-2} and that for (Ph)(Me)$_2$COOH = 5.43×10^{-2}). The values for the derived constants are given in Table I.

$$k_{ly} = k_aK_a/(K_a + a_H) \quad (2)$$

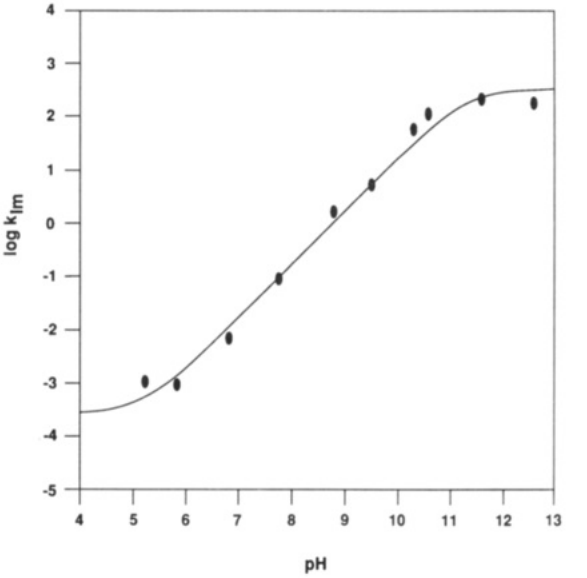

Figure 2. The pH dependence of the log of the rate constants (k_{Im}) for the reaction of (**1**)$Mn^{III}(X)$(ImH) with *t*-BuOOH. The points are experimentally determined rate constants for $ABTS^{\cdot+}$ formation (30 °C; μ = 0.2 in $NaNO_3$) and the curve was generated from eq 3. The values of constants that provided the optimal fits are provided in Table II.

Table II. Values of Rate and Equilibrium Constants Obtained from the Fitting of Equation 3 to the Experimental Points in Figure 2 (30 °C and μ = 0.2 with $NaNO_3$)

equiv kinetic terms	values
k_b (M^{-1} s^{-1})	2.74×10^{-4}
K_B (M^{-1})	5.01×10^{-9}
k_cK_B (s^{-1})	1.56×10^{-19}
k_dK_D (s^{-1})	1.75×10^{-9}
K_D (M^{-1})	5.01×10^{-12}

Kinetic studies on the reactions of (1)$Mn^{III}(X)_2$ with *t*-BuOOH in the presence of sufficient imidazole (ImH) to provide (1)$Mn^{III}(X)$(ImH) (established from a previous study[8]) were carried out in the pH range 5.3–12.6 (30 °C; μ = 0.2 with $NaNO_3$). A typical reaction mixture contained a buffered solution of 1.0×10^{-2} M ABTS, 5.2×10^{-3} M ImH, and (**1**)$Mn^{III}(X)_2$ in concentrations ranging from 5.0×10^{-6} to 1.0×10^{-4} M. Reactions were initiated by addition of an aqueous solution of *t*-BuOOH to a final concentration of 1.5×10^{-4} M. At all pH values examined the apparent first-order rate constants (k_{obsd}) for *t*-BuOOH disappearance were obtained from the fitting of the changes in absorbance to the rate expression for two sequential first-order reactions (ABTS → $ABTS^{\cdot+}$ → $ABTS^{2+}$).[8] The fitting of the kinetic data was carried out using five to six concentrations of (**1**)$Mn^{III}(X)$(ImH) at each pH value, and in each case k_{obsd} was found to be linearly dependent on [(**1**)$Mn^{III}(X)$(ImH)]. The second-order rate constants (k_{Im}) were taken as the slopes of the linear plots of k_{obsd} vs [(**1**)$Mn^{III}(X)$(ImH)].

The log k_{Im} vs pH profile for the reaction of *t*-BuOOH with (**1**)Mn^{III}(ImH)(X) is shown in Figure 2. The experimental points were fit to the empirical eq 3 (standard error = 2.07×10^{-1}). The values for the derived constants are given in Table II.

$$k_{Im} = \frac{k_ba_H}{(K_B + a_H)} + \frac{k_cK_Ba_H}{(a_H^2 + K_Ba_H + K_BK_D)} + \frac{k_dK_D}{(K_D + a_H)} \quad (3)$$

The Products Obtained from the Reaction of *t*-BuOOH (2.7×10^{-3} M) with (1)$Mn^{III}(X)_2$ (7.5×10^{-4} M) Were Determined in the Presence of ImH (5.2×10^{-2} M) and in Its Absence. The

Scheme II

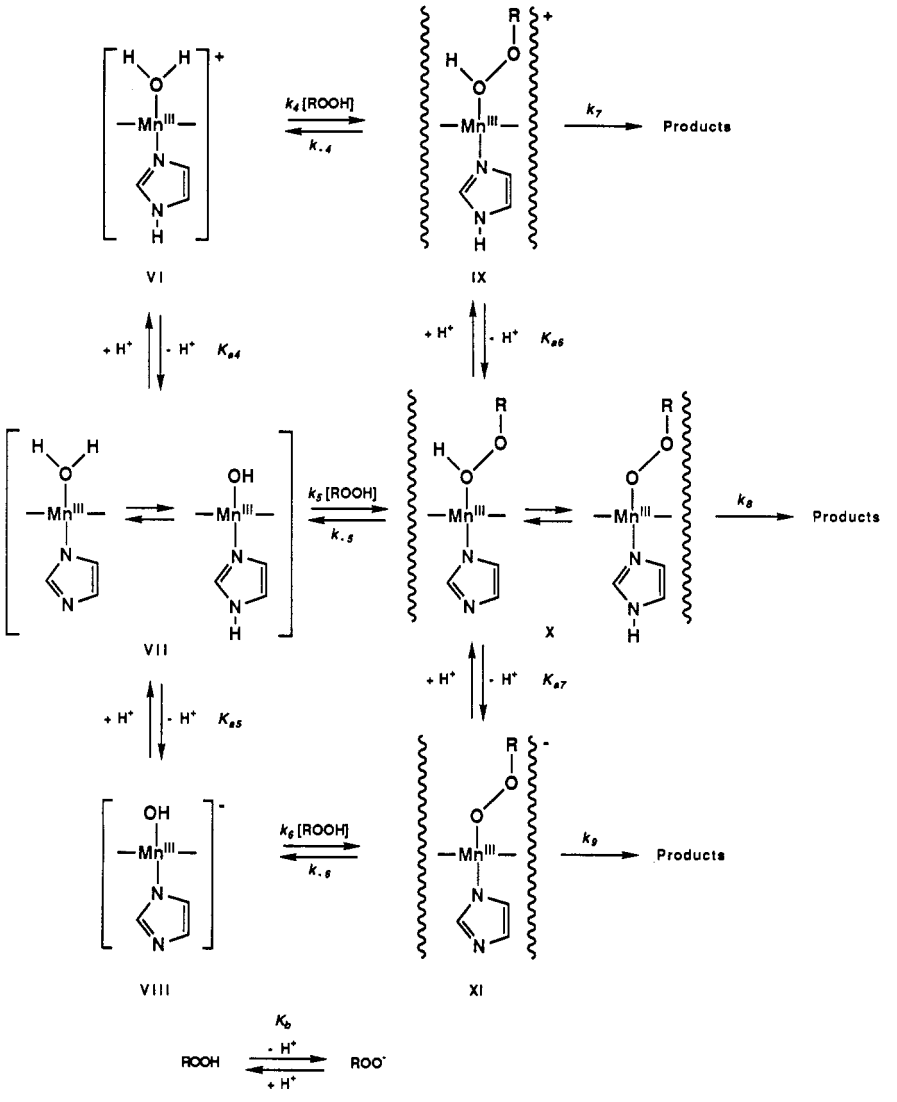

Table III. Percentage Yields of Products from the Reaction of *t*-BuOOH with (**1**)$Mn(X)_2$ in the Presence and Absence of Imidazole in Aqueous Solution {[(**1**)$Mn(X)_2]_i$ 7.5 × 10^{-4} M, $[t\text{-BuOOH}]_i$ = 2.7 × 10^{-3} M, and [ImH] = 5.0 × 10^{-2} M}

reaction conditions	yields of products,[a] %					
	t-BuOH	$(Me)_2CO$	*t*-BuOOMe	$(t\text{-BuO})_2$	MeOH	HCHO
pH 10.0, with ABTS in air	89	5				n.d.[b]
pH 10.0, with no ABTS in air	12	60	25	3	15	29
pH 10.0, with no ABTS under N_2	14	59	33		9	
pH 12.6, with no ABTS in air	11	70	22	trace	6	
pH 7.8, with ImH and no ABTS in air	19	67	13	1	4	24
pH 10.0, with ImH and no ABTS in air	19	63	16		13	10
pH 12.6, with ImH and no ABTS in air	63	34	4	1		5
pH 10.0, with ImH and ABTS in air	96	4			2	n.d.[b]
pH 12.6, with ImH and ABTS in air	85	5		2		n.d.[b]

[a] Based on *t*-BuOOH. [b] Not detected. Interference from $ABTS^{\cdot+}$ absorptions made colorimetric determination of HCHO difficult.

reactions were carried out using a higher oxidant concentration than that used for the kinetic studies in order to increase the concentrations of the products. In a typical reaction the reactants were combined, shaken thoroughly and allowed to stand for ~1.5 h before product analysis. Analysis of the spent reaction solutions was carried out by direct on-column injection to a GC {SGE, QC3/BP-1 (25 × 0.32 mm i.d.) capillary column as described by Lindsay Smith and Lower[17]}. For the anaerobic reactions, all the reagent solutions were thoroughly degassed with oxygen-free nitrogen gas and the reactions carried out in vials sealed with Teflon-lined crimp caps.

The products were identified as $(Me)_2CO$, *t*-BuOH, *t*-BuOOMe, $(t\text{-BuO})_2$, MeOH, and HCHO. All products were analyzed by GC, except for HCHO which was determined colorimetrically by the method described by Nash.[12] The product yields under the different experimental conditions are given in Table III. In every case the product balances were excellent and no major product remained undetected.

The pH Dependence of the Electrode Potentials for Oxidation and Reduction of (1)$Mn^{III}(X)$(ImH) in Water Solvent. Cyclic voltammetry of (**1**)$Mn^{III}(X)_2$ in the presence of sufficient imidazole to provide (**1**)$Mn^{III}(X)$(ImH) was carried out in aqueous solution (μ = 0.2 in $NaNO_3$, argon atmosphere) between pH 2 and 12 scanning with a glassy carbon electrode at 0.1 V/s. The cyclic

(12) Nash, T. *J. Biochemistry* **1953**, *55*, 416.

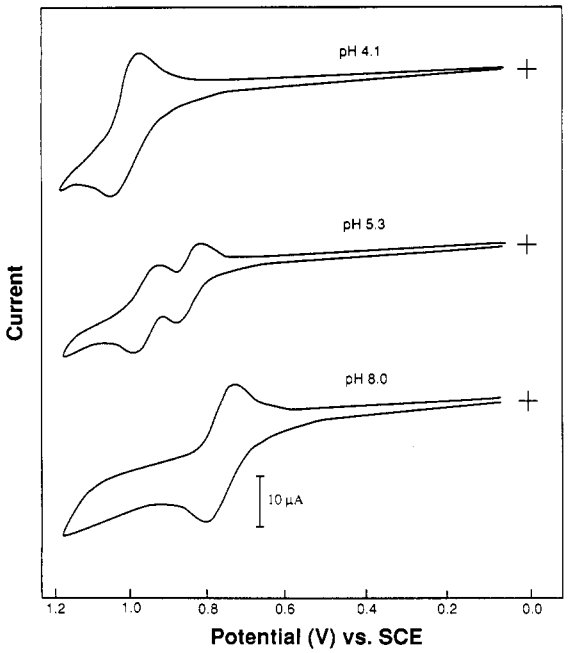

Figure 3. Cyclic voltammograms of (1)$Mn^{III}(X)_2$ in the presence of imidazole in water solvent (μ = 0.2 in $NaNO_3$) at pH 4.1, 5.3, and 8.0 (scan rate = 0.1 V/s).

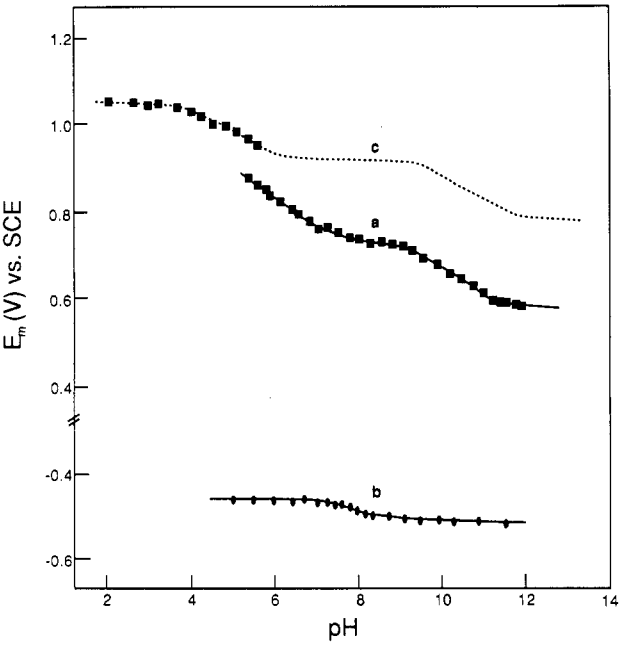

Figure 4. Nernst–Clark plots of the various midpoint potentials vs pH. The lines represent theoretical fits to the experimental points: (a) one-electron oxidation of (1)$Mn^{III}(X)$(ImH) to (1)$Mn^{IV}(X)$(ImH); (b) one-electron reduction of (1)$Mn^{III}(X)$(ImH) to (1)$Mn^{II}(X)$(ImH); (c) one-electron oxidation of (1)$Mn^{III}(X)_2$ to (1)$Mn^{IV}(X)_2$.

voltammograms (Figure 3) show that two oxidation waves are observed around pH 5. The sum of the wave-heights for these two waves equals the wave-height for a single $1e^-$ transfer process. Moreover, the midpoint potentials (E_m) measured below pH 5 were found to be the same for (1)$Mn^{III}(X)_2$ in the absence and presence of ImH. These observations imply that ImH ligates to (1)$Mn^{III}(X)_2$ only above pH 5. This was confirmed by UV/visible studies where spectral changes consistent with imidazole ligation were observed only above pH ~5. The midpoint potential for $1e^-$ oxidation of (1)$Mn^{IV}(X)$(ImH) could not be determined due to the intervention of the imidazole envelope.

The pH dependence of various midpoint potentials is shown in the Nernst–Clark plots of Figure 4. The midpoint potential for the first oxidation of (1)$Mn^{III}(X)$(ImH) shifts from +0.87 V at about pH 5 to +0.59 V above pH 12 as shown by trace **a** of Figure 4. Examination of trace **a** in Figure 4 shows two plateau regions, one with E_m = 0.73 V around pH 8, and a second with E_m = 0.59 V above pH 11.5. Between pH 5–7.5 and pH 9–11.5, the midpoint potential decreases with a slope of ~60 mV/pH indicating that a proton dissociation accompanies one-electron transfer. Traces **a** and **c** of Figure 4 compare the pH dependence of the midpoint potentials for the first oxidation of (1)$Mn^{III}(X)$(ImH) and (1)$Mn^{III}(X)_2$, respectively. The data points of Figure 4 are experimental while the lines were generated by computer fitting the appropriate Nernst–Clark equation (see Discussion section).

The midpoint potential for the first reduction of (1)$Mn^{III}(X)$(ImH) shifts from −0.46 to −0.50 V between pH 7 and 8 (trace **b** of Figure 4). Two plateau regions are observed between pH 5 and 12, one with a potential of −0.46 V between pH 5 and 7, and a second with a potential of −0.50 V between pH 8 and 12. The midpoint potential decreases with a slope of about 56 mV/pH between pH 7 and 8. Above pH 8 the E_m of $1e^-$ reduction of (1)$Mn^{III}(X)_2$ and (1)$Mn^{III}(X)$(ImH) differs by 40 mV.

Discussion

The present report describes a study on the kinetics and products of the reaction of (1)$Mn^{III}(X)_2$ with *t*-BuOOH and (Ph)$(Me)_2$COOH in water (pH 7.3–12.6, 30 °C with μ = 0.2 ($NaNO_3$)) in the presence of imidazole and in its absence. The findings strongly indicate that regardless of the pH employed (1)$Mn^{III}(X)_2$ catalyzes the homolytic scission of hydroperoxides in the absence of imidazole. In the presence of imidazole, however, the mechanism was found to be dependent on pH. Further, the dynamics for the reactions have been determined with *t*-BuOOH and (Ph)$(Me)_2$COOH and compared to those of $(Ph)_2$(MeOCO)COOH from a previous investigation.[8] The pH dependence of the second-order rate constants has been compared to the pH dependence of catalyst oxidation potential.

The pH dependences of the second-order rate constants (k_{ly}) for the reaction of *t*-BuOOH and (Ph)$(Me)_2$COOH with (1)$Mn^{III}(X)_2$ (from this study) and of $(Ph)_2$(MeOCO)COOH (from a previous study[8]) are shown in Figure 1. The data points in Figure 1 are experimental while the lines were generated from the empirical eq 1 which was derived from the reaction sequences of Scheme I. The development of the equation has been discussed in a previous paper[8] which assumes steady state conditions for intermediates IV and V. In the pH range 7.3–12.6, the reaction proceeds through the pathway shown in eq 4. The derived values

$$(1)Mn^{III}(OH)(H_2O) \underset{k_{-1}}{\overset{k_1[ROOH]}{\rightleftharpoons}} IV \underset{+H^+}{\overset{K_{a3}\ -H^+}{\rightleftharpoons}} V \xrightarrow{k_3} \text{Products} \quad (4)$$

of constants are reported in Table I. The thermodynamic constants K_{a1} and K_{a2} for the H^+ dissociation of the H_2O ligands of (1)$Mn^{III}(H_2O)_2$ have been previously determined (pK_{a1} = 5.8 and pK_{a2} = 12.2).[13]

The kinetic data obtained for the reactions of *t*-BuOOH, (Ph)$(Me)_2$COOH, and $(Ph)_2$(MeOCO)COOH may be compared by examining at any given pH the relationship between the log k_{ly} and the pK_a of the corresponding alcohol. If the hydroperoxide O–O bond cleavage was heterolytic the direct product of the reactions with (1)$Mn^{III}(X)_2$ would be the corresponding alcohols or alkoxides. Thus, at any given pH, one would expect a linear relationship between the pK_a values of the alcohols and the log k_{ly} values, where the order of the rate constants for the cleavage step would be $(Ph)_2$(MeOCO)COOH ≫ (Ph)$(Me)_2$COOH > *t*-BuOOH. The calculated pK_a values for $(Ph)_2$(MeOCO)COH, (Ph)$(Me)_2$COH, and *t*-BuOH are 11.1, 15.5, and 16.7, respectively.[9j] In the case of homolytic cleavage of the O–O bond the rate constants would not be expected to show significant dependency on the pK_a values of the alcohols and would be expected to be much the same.

(13) Kaaret, T. W.; Zhang, G. H.; Bruice, T. C. *J. Am. Chem. Soc.* **1991**, *113*, 4652.

Examination of the pH–rate profiles for *t*-BuOOH, (Ph)(Me)$_2$COOH, and (Ph)$_2$(MeOCO)COOH in Figure 1 shows that the profiles are very similar. Moreover, the second-order rate constants (k_{ly}) for the reactions exhibit only a modest dependency on the acidity of the ROH leaving group (β_{lg} = −0.32 between pH 7.3 and 10.0). These findings contrast markedly from the known heterolytic reactions involving (TPP)Mn^{III}(Cl) (TPP = dianion of *meso*-tetraphenylporphyrin) with various acyl hydroperoxides in benzonitrile where the log k_{ly} values show an inordinate sensitivity toward the pK_a of the leaving group (β_{lg} = −1.25).[14] Similar observations have been made with aqueous (**1**)Fe^{III}(X)$_2$ where the β_{lg} for the reactions with alkyl hydroperoxides was −0.11 while that for acyl hydroperoxides was −0.36 at neutral pH. This change in the value of β_{lg} upon moving from acyl to alkyl hydroperoxides has been attributed to a change in mechanism of the O–O bond cleavage of iron(III) porphyrin-bound hydroperoxide (i.e. from heterolytic to homolytic).[9f] The dependency of the log k_{ly} values of (**1**)Mn^{III}(X)$_2$ on the acidity of the ROH leaving group of *t*-BuOOH, (Ph)(Me)$_2$COOH, and (Ph)$_2$(MeOCO)COOH supports a homolytic mechanism for O–O bond cleavage of the manganese–porphyrin-bound alkyl hydroperoxide.

The products of the reaction of (1)Mn^{III}(X)$_2$ with *t*-BuOOH in the presence of the trapping agent ABTS (3.0×10^{-2} M) have been determined to be *t*-BuOH, (Me)$_2$CO, and MeOH (Table III). At pH 10.0, with [*t*-BuOOH]$_i$ = 2.7×10^{-3} M, the major product was *t*-BuOH (89%) while (Me)$_2$CO and MeOH were found only in very small amounts (5% and 4%, respectively). The observed product yields in the presence of an excess of ABTS may be accounted for by a mechanism involving the homolytic cleavage of the O–O bond of manganese-coordinated hydroperoxide to provide a *t*-BuO$^\bullet$ radical and a manganese(IV) porphyrin (eq 5). Thus the ABTS trapped intermediates would be (**1**)Mn^{IV}(OH)(X)

$$(\mathbf{1})\mathrm{Mn^{III}(X)}(t\text{-BuOOH}) \rightarrow (\mathbf{1})\mathrm{Mn^{IV}(OH)(X)} + t\text{-BuO}^\bullet + \mathrm{H^+} \quad (5)$$

and *t*-BuO$^\bullet$. This mechanistic pathway explains the predominant formation of *t*-BuOH as due to the reductive trapping of *t*-BuO$^\bullet$ by ABTS. However, 5% of the *t*-BuOOH reacting with (**1**)Mn^{III}(X)$_2$ is not trapped by ABTS resulting in the production of (Me)$_2$CO. This observation may be explained by an initial formation of a solvent-caged [manganese(IV) porphyrin $^\bullet$OBu-*t*] intermediate (eqs 7 and 8, Scheme III) where the *t*-BuO$^\bullet$ radicals occurring within the solvent cage are not subject to trapping while the solvent separated *t*-BuO$^\bullet$ radicals are subject to trapping. Thus, 5% of the *t*-BuO$^\bullet$ radicals that are formed undergo fragmentation within the solvent cage before being trapped by ABTS. The products formed through the solvent caged species are (Me)$_2$CO and Me$^\bullet$ (eq 7, Scheme III).

The major product of the reaction of (**1**)Mn^{III}(X)$_2$ with *t*-BuOOH in the absence of ABTS was determined to be (Me)$_2$CO. The remainder of the oxidant was recovered as *t*-BuOH, *t*-BuOOMe, (*t*-BuO)$_2$, MeOH, and HCHO. As shown in Table III, under these conditions the product distributions showed no significant dependence on the pH of the reaction solutions. The observed products may be explained by the series of reactions shown in Scheme III. At pH 10.0 and 12.6, with [*t*-BuOOH]$_i$

Scheme III

$$(\mathbf{1})\mathrm{Mn^{III}(H_2O)(L)} + t\text{-BuOOH} \longrightarrow (\mathbf{1})\mathrm{Mn^{III}(L)}(t\text{-BuOOH}) \quad (6)$$

$$(\mathbf{1})\mathrm{Mn^{III}(L)}(t\text{-BuOOH}) \longrightarrow \{(\mathbf{1})\mathrm{Mn^{IV}(O)(L)}\ ^\bullet\mathrm{OBu}\text{-}t\}_{cage} \rightarrow (\mathbf{1})\mathrm{Mn^{IV}(O)(L)} + (\mathrm{CH_3})_2\mathrm{CO} + \mathrm{CH_3}^\bullet \quad (7)$$

$$\{(\mathbf{1})\mathrm{Mn^{IV}(O)(L)}\ ^\bullet\mathrm{OBu}\text{-}t\}_{cage} \rightarrow (\mathbf{1})\mathrm{Mn^{IV}(O)(L)} + t\text{-BuO}^\bullet \quad (8)$$

$$(\mathbf{1})\mathrm{Mn^{IV}(O)(L)} + t\text{-BuOOH} \longrightarrow (\mathbf{1})\mathrm{Mn^{III}(OH)(L)} + t\text{-BuOO}^\bullet \quad (9)$$

$$t\text{-BuO}^\bullet + t\text{-BuOOH} \longrightarrow t\text{-BuOH} + t\text{-BuOO}^\bullet \quad (10)$$

$$2\ t\text{-BuOO}^\bullet \longrightarrow [t\text{-BuO}_4\text{Bu}\text{-}t] \longrightarrow [t\text{-BuO}^\bullet\mathrm{O_2}^\bullet\mathrm{OBu}\text{-}t]_{cage} \rightarrow 2\ t\text{-BuO}^\bullet + \mathrm{O_2} \quad (11)$$

$$[t\text{-BuO}^\bullet\mathrm{O_2}^\bullet\mathrm{OBu}\text{-}t]_{cage} \rightarrow t\text{-BuOOBu}\text{-}t + \mathrm{O_2} \quad (12)$$

$$t\text{-BuO}^\bullet \longrightarrow (\mathrm{CH_3})_2\mathrm{CO} + \mathrm{CH_3}^\bullet \quad (13)$$

$$t\text{-BuOO}^\bullet + \mathrm{CH_3}^\bullet \longrightarrow t\text{-BuOOCH}_3 \quad (14)$$

$$(\mathbf{1})\mathrm{Mn^{IV}(O)(L)} + \mathrm{CH_3}^\bullet + \mathrm{H^+} \longrightarrow \mathrm{CH_3OH} + (\mathbf{1})\mathrm{Mn^{III}(L)} \quad (15)$$

$$(\mathbf{1})\mathrm{Mn^{III}(OH)(L)} + \mathrm{CH_3}^\bullet \longrightarrow \mathrm{CH_3OH} + (\mathbf{1})\mathrm{Mn^{II}(L)} \quad (16)$$

(L = H_2O, HO^- or ImH)

Scheme IV

$$(\mathbf{1})\mathrm{Mn^{III}(X)_2} + t\text{-BuOOH} \longrightarrow (\mathbf{1})\mathrm{Mn^{V}(O)(X)} + t\text{-BuOH}$$

$$(\mathbf{1})\mathrm{Mn^{V}(O)(X)} + t\text{-BuOOH} \longrightarrow (\mathbf{1})\mathrm{Mn^{IV}(OH)(X)} + t\text{-BuOO}^\bullet$$

$$2\ t\text{-BuOO}^\bullet \longrightarrow [t\text{-BuO}_4\text{Bu}\text{-}t] \longrightarrow [t\text{-BuO}^\bullet\mathrm{O_2}^\bullet\mathrm{OBu}\text{-}t]_{cage} \rightarrow 2\ t\text{-BuO}^\bullet + \mathrm{O_2}$$

$$[t\text{-BuO}^\bullet\mathrm{O_2}^\bullet\mathrm{OBu}\text{-}t]_{cage} \rightarrow t\text{-BuOOBu}\text{-}t + \mathrm{O_2}$$

$$t\text{-BuO}^\bullet \longrightarrow (\mathrm{CH_3})_2\mathrm{CO} + \mathrm{CH_3}^\bullet$$

$$(\mathbf{1})\mathrm{Mn^{IV}(O)(X)} + \mathrm{CH_3}^\bullet + \mathrm{H^+} \longrightarrow \mathrm{CH_3OH} + (\mathbf{1})\mathrm{Mn^{III}(X)}$$

$= 2.7 \times 10^{-3}$ M, the $(Me)_2CO$ was formed in 60–70% yield arising from the β-scission of the *t*-BuO• radicals (eq 13). Under these conditions *t*-BuOH is only a minor product (~12%). The formation of *t*-BuOH may be explained by the reaction of the *t*-BuO• radicals with *t*-BuOOH (eq 10). The Me• radicals formed in eq 13 may react further to provide *t*-BuOOMe (25%) through the recombination of *t*-BuOO• with Me• (eq 14) and the mono-carbon products MeOH (eq 15) and HCHO (eq 19). When the reactions were carried out under anaerobic conditions there is a modest but significant increase in the yield of *t*-BuOOMe with a concomitant lowering in the yields of HCHO, MeOH, and $(t\text{-BuO})_2$. These observations support eq 14 over eqs 17 and 18. Additionally, small

$$Me^{\bullet} + O_2 \rightarrow MeOO^{\bullet} \quad (17)$$

$$MeOO^{\bullet} + t\text{-}BuOO^{\bullet} \rightarrow [t\text{-}BuO_4Me]_{cage} \rightarrow t\text{-}BuOOMe + O_2 \quad (18)$$

amounts of $(t\text{-BuO})_2$ were also observed. The most likely route leading to the formation of $(t\text{-BuO})_2$ is the self-reaction of *t*-BuOO• radicals (eq 12). In this context, the alternative combination of two *t*-BuO• radicals to provide $(t\text{-BuO})_2$ has been shown to be unimportant in solution.[14,15]

The reaction leading to the formation of HCHO is attributed to a methylperoxy–manganese(III) porphyrin which undergoes the elimination reaction of eq 19. This is similar to that proposed by Balch and co-workers[16] for the decomposition of alkylperoxo

$$(1)Mn^{III}O_2Me \rightarrow (1)Mn^{III}OH + HCHO \quad (19)$$

complexes of iron(III) porphyrins. Further, the same reaction has been invoked by Lindsay Smith and Lower[17] to describe the origin of HCHO in the reactions of [tetrakis(*N*-methyl-4-pyridyl)porphinato]iron(III) pentachloride with *t*-BuOOH in aqueous solution. Likely paths for the formation of the methylperoxy–manganese(III) porphyrin are given in eqs 20–25. A route for the formation of $(1)Mn^{II}$ is described by eq 16 in Scheme III.

$$(1)Mn^{II} + Me^{\bullet} \rightarrow (1)Mn^{III}Me \quad (20)$$

$$(1)Mn^{III}Me + O_2 \rightarrow (1)Mn^{III}O_2Me \quad (21)$$

$$Me^{\bullet} + O_2 \rightarrow MeO_2^{\bullet} \quad (22)$$

$$MeO_2^{\bullet} + (1)Mn^{II} \rightarrow (1)Mn^{III}O_2Me \quad (23)$$

$$(1)Mn^{II} + O_2 \rightarrow (1)Mn^{III}O_2^{\bullet} \quad (24)$$

$$(1)Mn^{III}O_2^{\bullet} + Me^{\bullet} \rightarrow (1)Mn^{III}O_2Me \quad (25)$$

Thus, the product studies clearly support a mechanism involving the homolytic cleavage of the O–O bond of manganese-coordinated alkyl hydroperoxide. The simplest presentation of a heterolytic mechanism for O–O bond cleavage should provide at least 50% *t*-BuOH (Scheme IV). If one includes a single cycle of eqs 10, 11, and 12 to Scheme IV, then the yield of *t*-BuOH should increase to 75%. Hence, a heterolytic mechanism is incompatible with our experimentally observed yields of *t*-BuOH (~12%) and acetone (~60–70%). Scheme III correctly predicts the observed material balance at pH 10.0 and 12.6.

The Effect of Imidazole Ligation on the Reaction of (1)-$Mn^{III}(X)_2$ with *t*-BuOOH. Previous studies on the reactions with $(Ph)_2(MeOCO)COOH$ have established that at saturating concentrations of ImH the manganese porphyrin is present as the mono-ligated species $(1)Mn^{III}(X)(ImH)$.[15] The reaction of $(1)Mn^{III}(X)(ImH)$ with *t*-BuOOH is kinetically first-order in both components. The pH dependence of the second-order rate constants (k_{Im}) for the reaction is provided in Figure 2. The experimental points in Figure 2 were fit to the empirical eq 3 (developed as described in a previous paper[8]) using the derived constants in Table II. The proposed series of reactions which account for the pH dependence of k_{Im} are shown in Scheme II which assumes steady state conditions for intermediates IX, X, and XI.

A comparison of the second-order rate constants in the absence (k_{ly}) and presence of ImH (k_{Im}) shows that imidazole provides about ~4- to 10-fold rate enhancement. Reasons to be considered for the rate enhancement include general-base catalysis (eq 26, Scheme V) and ligation of ImH to the manganese ion (eq 27, Scheme V), or a combination of both effects. That the rate enhancement is due solely to ligation of imidazole (eq 27) is supported by studies with the sterically bulky and nonligating ligand 2,4,6-trimethylpyridine.[8] Addition of 2,4,6-trimethylpyridine was found to have no influence on the rate of the reaction. Additionally, when the reactions were carried out below saturation in ImH, k_{obsd} increased linearly with an increase in [ImH], while at saturating concentrations of ImH, k_{obsd} was found to be independent of [ImH].[8,15] This indicates that ImH does not act

Scheme V

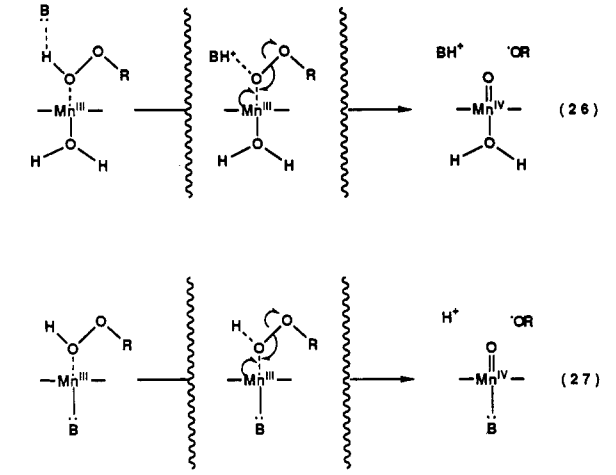

Scheme VI

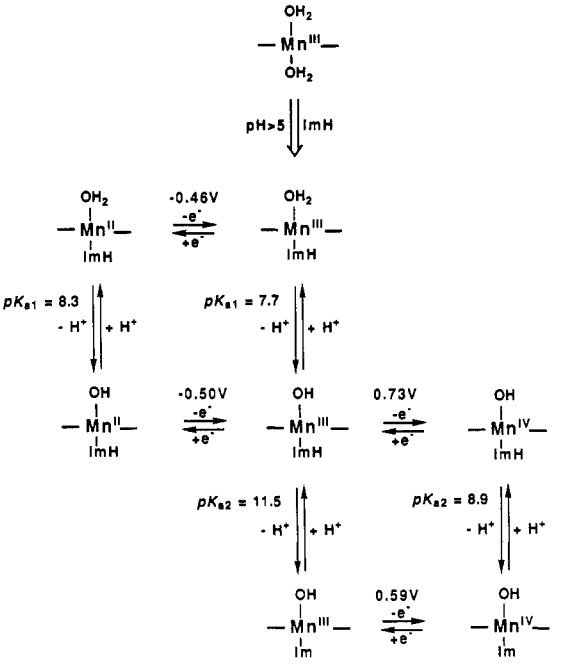

(14) Yuan, L. C.; Bruice, T. C. *Inorg. Chem.* **1985**, *24*, 986.
(15) Balasubramanian, P. N.; Schmidt, E. S.; Bruice, T. C. *J. Am. Chem. Soc.* **1987**, *109*, 7865.
(16) (a) Arasasingham, R. D.; Balch, A. L.; Latos-Grazynski, L. *J. Am. Chem. Soc.* **1987**, *109*, 5846. (b) Arasasingham, R. D.; Balch, A. L.; Latos-Grazynski, L. In *Studies in Organic Chemistry*; Ando, W., Moro-Oka, Y., Eds.; Elsevier: Amsterdam, The Netherlands, 1987; Vol. 33, p 417. (c) Arasasingham, R. D.; Balch, A. L.; Cornman, C. R.; Latos-Grazynski, L. *J. Am. Chem. Soc.* **1989**, *111*, 4357. (d) Arasasingham, R. D.; Cornman, C. R.; Balch, A. L. *J. Am. Chem. Soc.* **1989**, *111*, 7800. (e) Balch, A. L.; Hart, R. L.; Latos-Grazynski, L.; Traylor, T. G. *J. Am. Chem. Soc.* **1990**, *112*, 7382.
(17) Lindsay Smith, J. R.; Lower, R. J. *J. Chem. Soc., Perkin Trans. 2* **1991**, 31.

Scheme VII

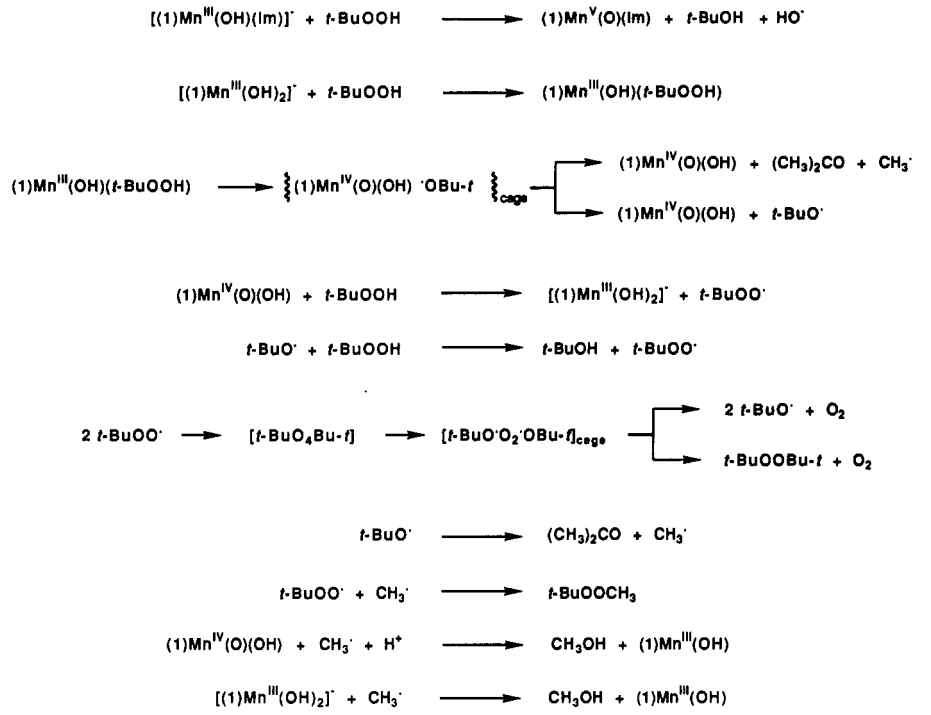

as a general-base catalyst in the reaction of (1)Mn^{III}(X)(ImH) with hydroperoxides. Thus the observed rate enhancement of the reactions in the presence of ImH arises due to the increased electron density at the metal center resulting from the donation of the lone pair electrons from the ligand.

Electrochemistry of (1)Mn^{III}(X)(ImH) in Water Solvent. The acid dissociation constants for (1)$Mn^{III}(H_2O)$(ImH) in aqueous solution were determined by electrochemical methods. The pH dependence of the electrode potentials of (1)Mn^{III}(X)(ImH) may be explained by the equilibria of Scheme VI. Plots of the midpoint potentials (E_m) as a function of pH for the electrode reactions of (1)Mn^{III}(X)(ImH) are shown in Figure 4. The points of Figure 4 are experimental while the solid lines were computer generated to fit the points using the appropriate Nernst–Clark equations (eqs 28 and 29) derived from Scheme VI. Thus the pH dependence of E_m (trace **a**, Figure 4) implies that the manganese(III) porphyrin in the presence of ImH exists as [(1)$Mn^{III}(H_2O)$(ImH)]$^+$, (1)Mn^{III}(HO)(ImH), and [(1)Mn^{III}(HO)(Im)]$^-$ dependent on pH. The pH dependence of E_m relates to the ionization of ligated H_2O or ImH and suggests a metal-centered oxidation. Equation 28 applies to the couple (1)Mn^{III}(X)(ImH)/(1)Mn^{IV}(X)(ImH), and the terms K_{a1}^{III}, K_{a2}^{III}, K_{a1}^{IV}, K_{a2}^{IV} are the first and second acid dissociation constants for (1)Mn^{III}(X)(ImH) and (1)Mn^{IV}(X)(ImH), respectively. Equation 29 applies for the couple (1)Mn^{III}(X)(ImH)/(1)Mn^{II}(X)(ImH).

$$E_m = E^{\circ\prime} + \frac{RT}{F} \ln \left[\frac{a_{H^+}^2 + K_{a1}^{III} a_{H^+} + K_{a1}^{III} K_{a2}^{III}}{a_{H^+}^2 + K_{a1}^{IV} a_{H^+} + K_{a1}^{IV} K_{a2}^{IV}} \right] \quad (28)$$

$$E_m = E^{\circ\prime} + \frac{RT}{F} \ln \left[\frac{a_{H^+} + K_{a1}^{II}}{a_{H^+}^2 + K_{a1}^{III} a_{H^+} + K_{a1}^{III} K_{a2}^{III}} \right] \quad (29)$$

The midpoint potentials at the two pH independent regions in the plot of E_m vs pH for 1e$^-$ oxidation of (1)Mn^{III}(X)(ImH) can be thought of as apparent formal potentials ($E^{\circ\prime}$) for [(1)Mn^{IV}(HO)(ImH)]$^+$ + e$^-$ → (1)Mn^{III}(HO)(ImH) and for (1)Mn^{IV}(HO)(Im) + e$^-$ → [(1)Mn^{III}(HO)(Im)]$^-$, respectively. The pH dependence of E_m for (1)Mn^{III}(X)(ImH) establishes the reduction as metal-centered to provide (1)Mn^{II}(X)(ImH).

The acid dissociation constants for (1)$Mn^{III}(H_2O)$(ImH), (1)$Mn^{IV}(H_2O)$(ImH), and (1)$Mn^{II}(H_2O)$(ImH), determined for the oxidation and reduction of (1)Mn^{III}(X)(ImH), are provided in Scheme VI. For comparison the acid dissociation constants (pK_{a1} and pK_{a2}) for (1)$Mn^{III}(H_2O)_2$ are 5.8 and 12.2, and for (1)$Mn^{IV}(H_2O)_2$ they are 4.4 and 9.9, respectively.[13]

The decrease of pK_{a1} with increase in the oxidation state of manganese is reasonable. Of considerable importance is the understanding that monoligated ImH or Im$^-$ serves as the axial ligand for manganese porphyrin derivatives at various oxidation states in aqueous solutions.

A comparison of the potentials for the 1e$^-$ oxidation of (1)Mn^{III}(OH)(ImH) (intermediate pH) and [(1)Mn^{III}(OH)(Im)]$^-$ (high pH) with (1)Mn^{III}(OH)(H_2O) and [(1)$Mn^{III}(OH)_2$]$^-$ shows that exchange of H_2O and HO$^-$ for ImH and Im$^-$, respectively, lowers the potential by 200 mV. This is equivalent to a change in free energy of activation ($\Delta\Delta G^{\ddagger}$) of ~4.6 kcal·mol^{-1}. However, such a large change in $\Delta\Delta G^{\ddagger}$ is not reflected in the ratio of the second-order rate constants for the reactions of (1)$Mn^{III}(X)_2$ with *t*-BuOOH which show at most a modest 10-fold rate enhancement upon ligation with imidazole. The more reactive $(Ph)_2$(MeOCO)COOH shows a somewhat greater rate enhancement of 100-fold upon imidazole ligation.[8] That the change in potential is not reflected completely in the change in rate constants is likely due to the inverse effect of increased electron density at the metal center on binding of *t*-BuOOH to the metal. In the case of the more electron deficient $(Ph)_2$(MeOCO)COOH the binding is more favored than *t*-BuOOH and thus a higher rate enhancement upon imidazole ligation is observed.

Products of the Reaction of (1)$Mn^{III}(X)_2$ with *t*-BuOOH in the Presence of ImH. When the reactions were carried out in the presence of ImH the product distribution showed significant dependence on the pH of the reaction mixtures as shown in Table III. Examination of Table III shows that at pH 7.8 and 10.0 (and omitting ABTS), the major product from *t*-BuOOH was $(Me)_2CO$ (63–67%), with the remainder being *t*-BuOH (19%), *t*-BuOOMe (13–16%), $(t\text{-BuO})_2$, MeOH, and HCHO. The product profiles observed here are consistent with a homolytic mechanism for the cleavage of the O–O bond. The series of reactions that account for these observations are similar to the reactions in the absence of imidazole and are shown in Scheme III.

Comparing the above reactions with that observed at pH 12.6 showed some important differences in the product distribution. At pH 12.6 there is a dramatic increase in the yield of *t*-BuOH (63%) with concomitant decreases in the yields of $(Me)_2CO$ (34%), *t*-BuOOMe (4%), HCHO, and MeOH. The observed increase

in the yield of *t*-BuOH at high pH may find explanation in a change in mechanism of the O–O bond cleavage from homolysis to heterolysis. We attribute this change at high pH to the proton dissociation of the manganese(III)-coordinated ImH {i.e., (**1**)-Mn^{III}(OOR)(ImH) → [(**1**)Mn^{III}(OOR)(Im)]$^-$, pK_a = 11.5}. Additionally, the formation of $(Me)_2CO$ (34%) and *t*-BuOOMe indicates that some homolysis also occurs. The products from homolysis may be explained by the reactions with [(**1**)Mn^{III}-$(OH)]_2^-$. Since at high pH (**1**)$Mn^{III}(X)_2$ does not completely saturate in Im^- due to the competition between HO^- and Im^- ligands, the reaction mixture would be expected to contain some $[(\mathbf{1})Mn^{III}(OH)]_2^-$. The series of reactions that account for these observations are shown in Scheme VII.

When the reactions were carried out with ABTS present in the reaction mixture the major product was *t*-BuOH with small amounts of $(Me)_2CO$ (5%). The formation of small amounts of $(Me)_2CO$ may once again find explanation in the solvent caged reaction of eq 7. In the presence of ABTS the product distributions were the same regardless of the pH employed.

Comparison of ImH and Im^- as Axial Ligands. The reaction properties of many metalloporphyrins are significantly influenced by the nature of the ligand trans to the reactive site. A change in the properties of the axially ligated imidazole ring by proton dissociation represents a mechanism whereby the electronic environment of the metal center can be altered. These observations are supported by UV/visible studies with (**1**)$Mn^{III}X_2$ which display differences in the visible absorption bands when Im^- is an axial ligand rather than ImH {λ_{max} for (**1**)Mn^{III}(X)(ImH): 374, 398, 423 (shoulder), 471 (Soret), 572, 608 nm; and λ_{max} for [(**1**)-Mn^{III}(X)(Im)]$^-$: 373, 398, 468 (Soret), 573, 609 nm}. Similarly, the electronic absorption bands for the related mono-imidazolate complex, [(P)Fe^{II}(CO)(Im)]$^-$ (P = dianion of protoporphyrin dimethyl ester or dianion of *meso*-tetraphenylporphyrin), occur at lower energy than those for the corresponding imidazole complex (P)Fe^{II}(CO)(ImH), and the binding affinity and rate constants for CO binding to [(P)Fe^{II}(Im)]$^-$ have been shown to be lower than those of the protonated (P)Fe^{II}(ImH).[18] Thus, the electronic properties of the proximal ligand in many hemeproteins may well contribute significantly to defining the catalytic characteristics of the enzyme. Indeed several investigators have suggested that a number of hemeproteins which contain a histidine residue as a proximal ligand may possess an imidazolate, rather than an imidazole, as an axial ligand.[18a,19]

Acknowledgment. This work was supported by a grant from the National Institutes of Health.

(18) (a) Mincey, T.; Traylor, T. G. *J. Am. Chem. Soc.* **1979**, *101*, 765. (b) Stanford, M. A.; Swartz, J. C.; Phillips, T. E.; Hoffman, B. M. *J. Am. Chem. Soc.* **1980**, *102*, 4492. (c) Swartz, J. C.; Stanford, M. A.; Noy, J. N.; Hoffman, B. M.; Valentine, J. S. *J. Am. Chem. Soc.* **1979**, *101*, 3396.

(19) (a) Peisach, J.; Blumberg, W. E.; Adler, A. *Ann. N.Y. Acad. Sci.* **1973**, *206*, 310. (b) Peisach, J. *Ann. N.Y. Acad. Sci.* **1975**, *244*, 187. (c) Peisach, J.; Mims, W. B. *Biochemistry* **1977**, *16*, 2795. (d) Morrison, M.; Schonbaum, G. R. *Annu. Rev. Biochem.* **1976**, *45*, 861. (e) Brautigan, D. L.; Feinberg, B. A.; Hoffman, B. M.; Margoliash, E.; Peisach, J.; Blumberg, W. E. *J. Biol. Chem.* **1977**, *252*, 574. (f) Stein, P.; Mitchell, M.; Spiro, T. G. *J. Am. Chem. Soc.* **1980**, *102*, 7795.

Synthetic and Mechanistic Studies on the Antitumor Antibiotics Esperamicin A_1 and Calicheamicin γ_1: Synthesis of 2-Ketobicyclo[7.3.1] Enediyne and 13-Ketocyclo[7.3.1] Enediyne Cores Mediated by η^2 Dicobalt Hexacarbonyl Alkyne Complexes. Cycloaromatization Rate Studies

Philip Magnus,*,† Paul Carter,‡ Jason Elliott,‡ Richard Lewis,† John Harling,† Thomas Pitterna,† William E. Bauta,† and Simon Fortt†

Contribution from the Department of Chemistry and Biochemistry, University of Texas at Austin, Austin, Texas 78712, and Department of Chemistry, Indiana University, Bloomington, Indiana 47405. *Received August 26, 1991*

Abstract: A general strategy for the construction of the bicyclo[7.3.1]tridecenediyne core structure of the antitumor antibiotics esperamicin and calicheamicin can be realized provided the 10,11-acetylenic bond is complexed as its derived η^2 $Co_2(CO)_6$ adduct. The 10,11-η^2-2-ketobicyclo[7.3.1] enediyne dicobalt hexacarbonyl adduct **38** was synthesized using η^2 dicobalt hexacarbonyl propargyl cation alkylation to form the crucial 10-membered ring. Oxidative decomplexation of **38** in 1,4-cyclohexadiene gave the cycloaromatized adduct **49**, presumably via the uncomplexed 2-ketobicyclo[7.3.1] enediyne **27**. The keto isomer 10,11-η^2-13-ketobicyclo[7.3.1] enediyne dicobalt hexacarbonyl adduct **39** was synthesized in a similar manner and its structure secured by single-crystal X-ray crystallography. Oxidative decomplexation of **39** gave the 13-ketobicyclo[7.3.1] enediyne **32** as a stable crystalline solid. The five-membered-ring analogue, 12-ketobicyclo[7.2.1] enediyne **94**, was readily made in the same way. The relative rates of cycloaromatization of **32** compared to the derived alcohol **86** and the five-membered-ring analogue **94** (and **97**) demonstrate that the distance (*r*) between the bonding acetylenes (leading to the 1,4-diyl) in the ground state does not control the rate of cycloaromatization. Strain release in the transition state predicts the relative rates of cycloaromatization.

Introduction

During the past 40 years or so, cancer chemotherapy has relied upon natural product chemistry to provide so-called lead compounds and continues to do so.[1] In 1975 Ferguson aptly stated, "What is sorely needed is a good guide or rationale for planning the structure of an effective cytotoxic agent. This stage will come when we have an understanding of the mechanisms of action of antitumor drugs which in turn is fostered by having a working hypothesis for a mode of action of a given type of drug. Organic

†University of Texas at Austin.
‡Indiana University.

(1) *Anticancer Agents Based on Natural Product Models*; Medicinal Chemistry 16; Cassady, J. M., Douros, J. D., Eds.; Academic Press: New York, 1980.

0002-7863/92/1514-2544$03.00/0